DOI: 10.1002/adma.200602172

High-Efficiency and Stable Mesoscopic Dye-Sensitized Solar Cells Based on a High Molar Extinction Coefficient Ruthenium Sensitizer and Nonvolatile Electrolyte**

By *Daibin Kuang*, *Cedric Klein*, *Seigo Ito*, *Jacques-E. Moser*, *Robin Humphry-Baker*, *Nick Evans*, *Francine Duriaux*, *Carole Grätzel*, *Shaik M. Zakeeruddin*,* and *Michael Grätzel**

Solar energy is a renewable and clean energy source that is inexhaustible; about 3×10^{24} J can be supplied to the Earth from the Sun per year, or about 10 000 times more than the global population currently consumes.[1] Dye-sensitized solar cells (DSCs), which convert light to electricity by means of harvesting of solar irradiation by the sensitizer, have attracted considerable attention in scientific research and for practical applications. The intrinsic advantages of these devices are high photoelectrical efficiency over a large span of the visible light spectrum under direct sunlight and diffuse light conditions as well as low cost compared to the traditional solid-state crystalline silicon solar cells.[2–5]

In order to improve the photovoltaic performance and stability of DSCs, extensive efforts have been focused on the synthesis of new highly efficient sensitizers and the search for stable electrolytes and/or new photoanode materials.[6–10] In the last 15 years significant progress has been achieved in the optimization of the device performance and stability.[6] Recent studies have emphasized that sensitizers with high molar extinction coefficients are an effective means of augmenting the efficiency of thin-film dye-sensitized solar cells.[6a] A new series of these dyes with high molar extinction coefficients from the *cis*-RuLL′(SCN)$_2$ family, where L and L′ are substituted bipyridyl ligands featuring alkyl or ethylene oxide groups, have been synthesized and utilized in DSCs, revealing promising properties.[6] This Communication reports the synthesis of a new sensitizer, Ru(2,2′–bipyridine-4,4′-dicarboxylic acid)(4,4′-bis(2-(4-*tert*-butyloxyphenyl)ethenyl)-2,2′–bipyridine) (NCS)$_2$, denoted K77 (Fig. 1), which, used in combination with a newly designed nonvolatile electrolyte, exhibits a remarkable, unique performance combining high efficiency with excellent stability during long-term accelerated tests at both 80 °C in the dark and under light soaking at 60 °C.

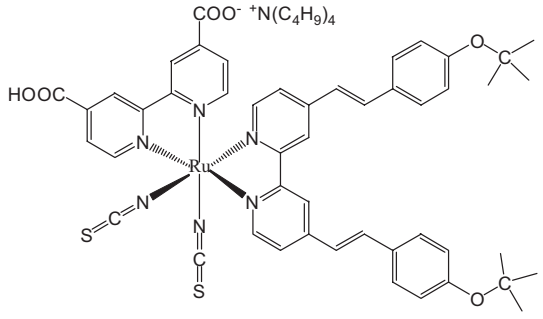

Figure 1. Molecular structure of the K77 sensitizer.

A cyclic voltammogram of the K77 dye anchored on a 6 μm thick mesoscopic TiO_2 film shows chemically reversible redox waves with the formal potential, $(E_{ox} + E_{red})/2$, appearing at 0.97 V versus NHE (normal hydrogen electrode), a potential value more positive than that of the redox mediator couple used in the electrolyte. The thermodynamic driving force for the regeneration of the K77 dye by iodide in the present nonvolatile organic electrolyte is 570 mV.

The UV-vis absorption and emission spectra of the K77 dye in dimethylformamide (DMF) solution are shown in Figure S1 (Supporting Information). The absorption spectrum has a peak corresponding to the lowest metal-to-ligand charge transfer (MLCT) absorption band at 546 nm with a molar extinction coefficient of 19.4×10^3 M^{-1} cm^{-1}. The absorption bands seen at 346 nm and 310 nm correspond to the π–π* transitions of 4,4′-bis(2-(4-*tert*-butyloxyphenyl)ethenyl)-2,2′-bipyridine and 2,2′-bipyridine-4,4′-dicarboxylic acid, respectively. The luminescence maximum is located at 800 nm. The E_{0-0} transition energy of the dye was estimated to be 1.75 eV from the absorption and emission spectra. The standard potential ($\phi^0(S^+/S^*)$ of the K77 dye can be calculated from the relation $\phi^0(S^+/S) = \phi^0(S^+/S^*) - E_{0-0}$, yielding –0.78 V versus NHE. Consequently, $\phi^0(S^+/S^*)$ of K77 is more negative (or higher in energy) than the conduction band edge of TiO_2, providing a thermodynamic driving force for electron injection from the dye to TiO_2.

[*] Dr. S. M. Zakeeruddin, Prof. M. Grätzel, Dr. D. Kuang, Dr. C. Klein, Dr. S. Ito, Prof. J.-E. Moser, Dr. R. Humphry-Baker, Dr. N. Evans, F. Duriaux, Dr. C. Grätzel
Laboratory for Photonics and Interfaces
Institute of Chemical Sciences and Engineering
Ecole Polytechnique Fédérale de Lausanne
1015 Lausanne (Switzerland)
E-mail: shaik.zakeer@epfl.ch; michael.graetzel@epfl.ch

[**] The present work is supported by The Swiss Science Foundation and the Swiss Commission of Technology and Innovation (CTI) under contract number 7019.1 NMS-NM. We thank Dr. Q. Wang for helpful discussions, P. Comte for the preparation of TiO_2 paste, and Dr. T. Koyanagi (CCIC, Japan) for a free sample of the 400 nm sized light-scattering particles. Supporting Information is available online from Wiley InterScience or from the author.

ADVANCED MATERIALS

The photovoltaic performance of DSCs is largely dependent on the kinetic competition between recapture of the injected electrons from the conduction band of the semiconductor electrode by oxidized dye (S^+) and the interception of the back electron transfer by regeneration of the sensitizer by the redox mediator. Hence, nanosecond laser transient absorbance measurements were performed to scrutinize the kinetics of these two charge-transfer processes for the K77 dye. In ruthenium(III) polypyridyl complexes containing thiocyanate ligands, the oxidized state (S^+) has a characteristic absorption at $\lambda > 620$ nm due to a ligand-to-metal charge-transfer transition (LMCT). In the absence of a redox mediator (i.e., in pure 3-methoxypropionitrile (MPN) solvent), the decay of the absorption signal recorded at $\lambda = 680$ nm reflects the dynamics of the recombination of injected electrons with the oxidized dye (S^+). Figure 2 shows that the transient absorbance of the oxidized state of the K77 dye decays with a typical half-reaction time $t_{1/2} = 180$ μs. Data could be fitted by single exponentials, yielding a rate constant of $k_b = 3.7 \times 10^3$ s^{-1}. In the presence of the iodide/triiodide redox couple the decay of the oxidized dye signal was significantly accelerated, the half-reaction time decreasing to $t_{1/2} = 8$ μs. Data could be fitted by single exponentials, resulting in a rate constant of $k_r = 1.0 \times 10^5$ s^{-1} for the regeneration process. This thirty-times-higher k_r value indicates that electron recombination with the oxidized dye state is indeed intercepted by the mediator, and that the sensitizer is efficiently regenerated by iodide.

Figure 3 is a typical photocurrent density–voltage (*J–V*) curve of the DSC device prepared with the K77 dye in combination with a volatile electrolyte (Z675). The corresponding photovoltaic parameters (short-circuit current density J_{sc}, open-circuit voltage V_{oc}, and fill factor *FF*) of the device with an active cell area of 0.158 cm^2 using a black metal mask under simulated air mass (AM) 1.5 sunlight at 1000 $W m^{-2}$ are $J_{sc} = 19.2$ mA cm^{-2}, $V_{oc} = 780$ mV, and $FF = 0.725$, resulting in 10.5 % power-conversion efficiency. Under low light intensity the photovoltaic performance was as high as 11.05 %. To avoid any light capture in the space between the cell and metal mask, a black tape was added, decreasing the nominal value of the photocurrent by 2–3 %. The photocurrent action spectrum of the device with K77 and the volatile electrolyte (Z675) is shown as an inset in Figure 3. The incident-photon-to-current conversion efficiency (IPCE) of this device exceeds 80 % in a broad spectral range from 470–670 nm, reaching its maximum of 90 % at 550 nm.

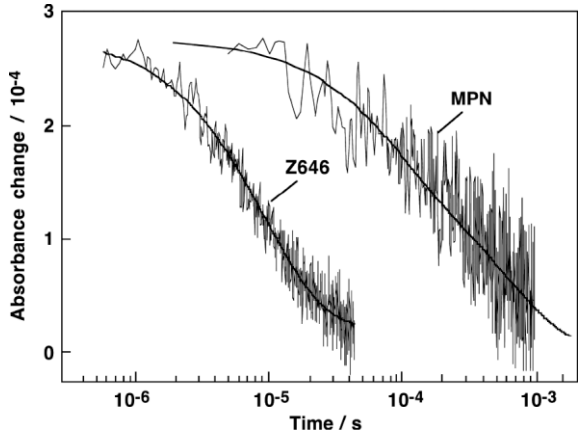

Figure 2. Transient absorbance decay kinetics of the oxidized state of K77 dye adsorbed on nanocrystalline TiO_2 films in pure MPN solvent and in nonvolatile electrolyte (Z646). Smooth solid lines are single exponential fits of experimental data with rate constants $k = 3.7 \times 10^3$ s^{-1} and $k = 1.0 \times 10^5$ s^{-1}, respectively. Absorbance changes were measured at a probe wavelength of 650 nm following 600 nm pulsed laser excitation (5 ns FWHM pulse duration, 20 μJ cm^{-2} pulse fluence, 30 Hz repetition rate). Signals shown were obtained by averaging typically over 3500 laser shots.

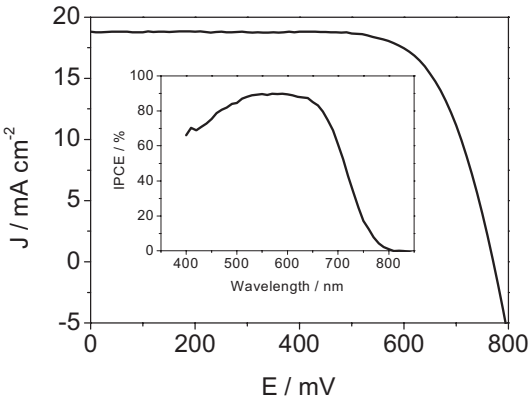

Figure 3. Photocurrent intensity–voltage characteristics of a DSC device based on the K77 sensitizer and volatile electrolyte (Z675), measured at air mass 1.5 (100 mW cm^{-2}) full sunlight illumination. Inset: Photocurrent action spectrum of the device.

Owing to the inherent difficulties of encapsulation of volatile organic solvents at higher temperatures, long-term thermal stability testing of the DSCs based on a newly formulated nonvolatile organic solvent electrolyte (Z646; composition stated in experimental section) was undertaken. The photovoltaic parameters J_{sc}, V_{oc}, *FF*, and η (power-conversion efficiency) for DSC devices in the presence of this nonvolatile electrolyte are 17.5 mA cm^{-2}, 737 mV, 0.696, and 9.0 %, respectively (Fig. S2, Supporting Information). The cells were measured following overnight visible-light soaking (AM 1.5) at 60 °C. The detailed photovoltaic parameters for different light intensities are shown in Table 1. One cell equipped with a reflecting Pt mirror counter electrode produced an even higher efficiency of 9.5 %, the photovoltaic parameters in AM 1.5 full sunlight being $J_{sc} = 17.9$ mA cm^{-2}, $V_{oc} = 745$ mV, and $FF = 0.711$. For this champion cell under low light intensity the photovoltaic performance was as high as 10 % efficiency. Using K19 dye and a similar nonvolatile electrolyte, 8 % efficiency (1 sun light intensity) was previously reported.[6d] Utilization of K77 dye thus results in a substantial improvement of efficiency compared to the earlier reported values with K19 dye. These reproducible improvements arise most likely from modifications made to the dye as well as to the electrolyte.

Table 1. Detailed photovoltaic parameters of the device based on K77 and the nonvolatile electrolyte (Z646) under various sunlight irradiation intensities [a].

Light intensity	J_{SC} [mA cm^2]	V_{OC} [mV]	*FF*	η [%]
1.0 sun	17.5	737	0.696	9.0
0.52 sun	9.38	720	0.729	9.3
0.3 sun	5.5	705	0.748	9.5

[a] The spectral distribution of the xenon lamp simulates air mass 1.5 solar light. 1.0 sun mismatch has been corrected to correspond to AM 1.5 global sunlight (100 mW cm^{-2}). The active area of the cell with a metal mask was 0.158 cm^2.

In order to match specifications required for practical applications to be implemented outdoors, light soaking and thermal stability tests of these DSCs devices, performed under realistic conditions and constraints, were carried out in the laboratory. The DSCs were covered with a 50 μm thick layer of polyester film acting as a UV cutoff filter (up to 400 nm) and subjected to accelerated testing in a solar simulator at 100 mW cm^{-2} (full sun) and 60 °C. Following the 1000 h light-soaking accelerated test, the measured DSC photovoltaic performance of 8.23 % revealed almost no change compared to the initial value (8.3 %). As shown in Figure 4, this relative cell stability (in terms of efficiency) was achieved by constancy in the photocurrent as well as compensation of the small voltage loss of 30 mV by an increase in *FF*.

These robust and high efficiency DSCs were further tested for long-term stability by subjecting them to high-temperature stress (i.e., 80 °C) in the dark. The photovoltaic parameter variations during this aging process include a slight 27 mV drop in photovoltage accompanied by a small photocurrent decay following the 1000 h accelerated test at 80 °C (Supporting Information, Fig. S3). The drop in current and voltage was compensated by an increase in *FF* (from 0.675 to 0.714). The photoelectric conversion efficiency retains more than 98 % of its initial value even after 1000 h of accelerated testing at 80 °C in the dark. The presently investigated system, based on the new nonvolatile electrolyte (Z646) in conjunction with the K77 sensitizer (and in the absence of co-adsorbent), is the most stable DSC device reported thus far.

Electrochemical impedance spectroscopy (EIS) was used to characterize the basic properties of the DSCs during long-term aging. Recently, new physical models have been developed and applied to the study of DSCs.[11,12] In order to understand the photovoltaic parameter variations during the aging processes of DSCs, EIS measurements were performed. This experimental technique allows the investigation of the electron recombination at the TiO_2/electrolyte interface, electron transport in the TiO_2 electrode, electron transfer at the counter electrode, and I_3^- transport in the electrolyte phase of the dye-sensitized solar cells.[11,12] Figure 5a and b displays the Bode phase and Nyquist plots of the DSC device (Z646 electrolyte) measured in the dark at –0.70 V bias for the fresh cell and after aging for 1000 h at 80 °C in the dark. The two maxima of the phase angles in the Bode phase plot shift to higher frequency, indicating that the interfacial electron transfer from both the dye-coated TiO_2 working electrode and the counter electrode is accelerated upon aging. A corresponding reduction in the radius of the semicircles is seen in the Nyquist plot. Using a previously developed model[11,12] to fit the data, the electron lifetime (τ) in the mesoscopic TiO_2 film,

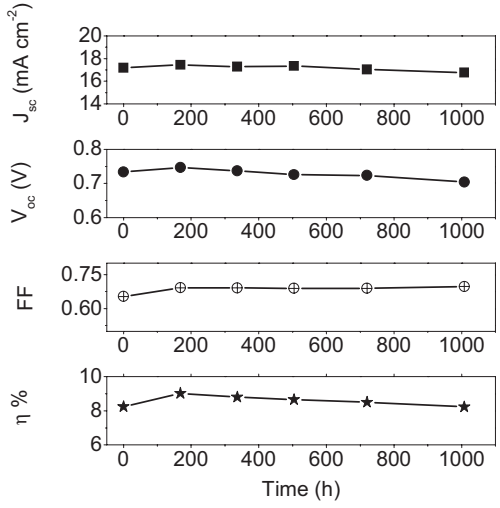

Figure 4. Stability test. Photovoltaic parameter (J_{sc}, V_{oc}, *FF*, and η) variations with aging time for the device based on K77 and the nonvolatile electrolyte (Z646) subjected to successive aging under light soaking at 60 °C.

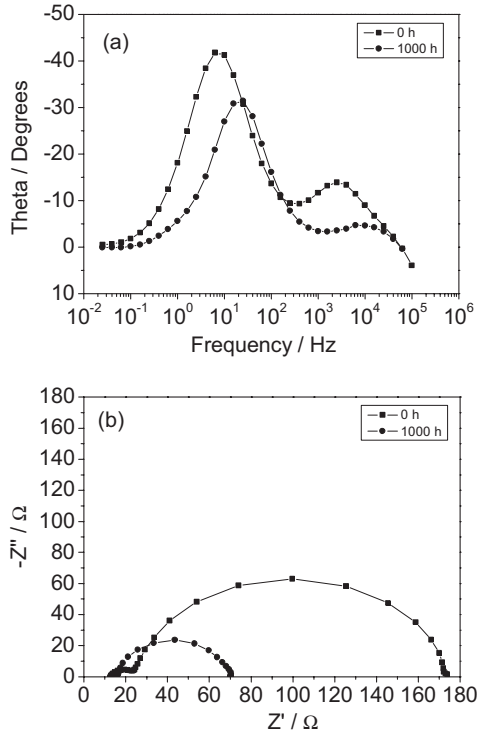

Figure 5. Impedance spectra measured at –0.7 V bias in the dark of DSC devices based on K77 and the nonvolatile electrolyte (Z646) for the fresh and aged cells following the accelerated test time (1000 h) at 80 °C in the dark. a) Bode phase plots, b) Nyquist plots.

ADVANCED MATERIALS

due to back reaction with I_3^-, decreases from 62.6 to 15.2 ms. These observations are consistent with an increase in the dark current measured under forward bias. The enhanced dark current and decrease in the calculated electron lifetime indicate that the conduction band edge of TiO_2 moves towards more positive potentials during aging, resulting in a lowering of the junction barrier. This conduction-band shift is consistent with the small drop in V_{oc} observed upon aging of the cells. The reasons for this displacement remain to be explored but a plausible hypothesis is that it relates to proton intercalation. The decrease in the electron transfer resistance for triiodide reduction at the counter electrode (i.e., high-frequency peak of the Bode phase plot shifting towards larger values) upon aging explains the observed increase of *FF* from 0.675 to 0.714.

In conclusion, mesoscopic dye-sensitized solar cells (DSCs) with more than a 10.5 % photoelectrical conversion efficiency were obtained utilizing the newly designed high molar extinction coefficient sensitizer (K77) in conjunction with a volatile electrolyte (Z675). Highly efficient DSCs (up to 9.5 %) exhibiting unprecedented long-term stability (1000 h) under both light soaking and thermal stressing have been obtained using the K77 sensitizer in combination with a newly formulated nonvolatile organic-solvent-based electrolyte (Z646).

Experimental

Reagents: 1-Propyl-3-methylimidazolium iodide (PMII) ionic liquid was prepared according to literature methods and the purity was confirmed by ^{1}H NMR spectra [13]. Guanidinium thiocyanate (GuNCS) was purchased from Fluka. 1-Butyl-1*H*-benzimidazole (NBB) was synthesized as given below.

*Synthesis of 1-Butyl-1*H*-benzimidazole*: A mixture of 1*H*-benzimidazole (9.45 g, 80.0 mmol), 1-bromobutane (13 cm^3, 0.12 mol), tetrabutylammonium bromide (1.3 g, 4.0 mmol), toluene (50 cm^3), and aqueous sodium hydroxide (33 %; 38 g) was stirred vigorously for 1 day at 60 °C. The mixture was cooled to room temperature, diluted with water (100 cm^3), and the aqueous layer extracted with dichloromethane (2 × 50 cm^3). The combined organic layers were dried with magnesium sulfate and evaporated under reduced pressure. The crude product was purified by dry flash chromatography on silica using diethyl ether as eluent for the impurities and ethyl acetate as eluent for the product. The product was further purified by Kugelrohr distillation (200 °C, 0.1 mmHg) to give 1-butyl-1*H*-benzimidazole (7.06 g, 51 %) as a clear colorless oil; R_f (ethyl acetate) 0.2; δ_H (400 MHz; *d*-chloroform) 0.98 (3H, t, *J* 7.4, CH_3), 1.34–1.45 (2H, m, CH_2), 1.85–1.94 (2H, m, CH_2), 4.20 (2H, t, *J* 7.1, NCH_2), 7.27–7.35 (2H, m, 2 × ArH), 7.40–7.45 (1H, m, ArH), 7.81–7.86 (1H, m, ArH), and 7.91 (1H, s, CH). The δ_H (*d*-chloroform) data are in agreement with literature data [14].

4,4′-Bis(2-(4-tert-butyloxyphenyl)ethenyl)-2,2′-bipyridine: Solid ^{t}BuOK (5 g, 44 mmol) was added to a solution of 4,4′-dimethyl-2,2′-bipyridine (2.1 g, 11 mmol) and 4-*tert*-butyloxybenzaldehyde (5 g, 28 mmol) in anhydrous DMF (120 mL). The resulting mixture was stirred for 24 h at room temperature under nitrogen. After evaporation of DMF, MeOH (200 mL) was added and the solid was filtered and washed with MeOH then cold acetone to afford 2.5 g (45 %) of the desired product as a white solid.

^{1}H NMR (200 MHz, 25 °C, $CDCl_3$) δ 1.40 (s, 18H), 7.06 (m, 6H), 7.46 (m, 8H), 8.54 (s, 2H), 8.67 (d, *J* = 5.5 Hz, 2H) ppm. ^{13}C NMR (50 MHz, 25 °C, $CDCl_3$) δ 28.9, 79.0, 118.1, 120.9, 124.1, 124.8, 127.7, 131.3, 132.9, 146.0, 149.5, 156.2, 156.5 ppm.

Synthesis of Ru(2,2′–bipyridine-4,4′-dicarboxylic acid-)(4,4′-bis(2-(4-tert-butyloxyphenyl)ethenyl)-2,2′–bipyridine) (NCS)$_2$: A mixture of 4,4′-bis(2-(4-*tert*-butyloxyphenyl)ethenyl)-2,2′-bipyridine (1 g, 1.98 mmol) and $(Ru(Cl)_2(p\text{-cymene}))_2$ (0.607 g, 0.99 mmol) in DMF (80 mL) was refluxed for 4 h under nitrogen. After this time, 4,4′-dicarboxy-2,2′-bipyridine (0.484 g, 1.98 mmol) was added to the reaction mixture and heated to 140 °C for 4 h under nitrogen in the dark. To the green mixture was then added NH_4NCS (2.3 g, 30 mmol), and heating was continued for 4 h. After the mixture had cooled to room temperature, DMF was evaporated and water (200 mL) was added. The resulting purple solid was filtered and washed with water. The crude complex was dissolved in basic methanol (TBAOH) and passed through a Sephadex LH 20 column with methanol as an eluent. The pure compound was collected and the pH lowered to 4.8 by titrating with dilute HNO_3. The obtained solid was washed with water and dried under vacuum. ^{1}H NMR (200 MHz, 25 °C, CD_3OD + NaOD) δ 9.45(d, 1H), 9.25(d, 1H), 8.95 (s, 1H), 8.8 (s, 1H), 8.35 (s, 1H), 8.2 (s, 1H), 8.0 (d, 1H), 6.7–7.9 (m, 17H), 4.4–1.0 (m, 54H) ppm. Anal. calc. for $RuC_{54}H_{55.5}N_6O_{12}S_2 \cdot H_2O$ (TBA): C 62.7, H 6.7, N 8.0 %. Found: C 61.5, H 6.5, N 8.4 %.

The characterization of the sensitizer (K77) was performed with ^{1}H NMR, elemental analysis, UV-vis, photoluminescence, Fourier transform infrared (FTIR), cyclic voltammetry, and nanosecond laser transient absorbance measurements. The experimental details are given in our previous publications [6]. Impedance spectra of DSCs were measured in the dark at –0.7 V applied forward bias using a potentiostat (EG&G, M273) equipped with a frequency response analyzer (EG&G, M1025). The spectra were scanned in the frequency range 0.005 Hz to 100 kHz at room temperature with alternating voltage amplitude set at 10 mV.

Preparation of Mesoscopic TiO_2 films: The mesoscopic TiO_2 films that were used as photoanodes consisted of double layers (6 + 4 μm). The detailed method of TiO_2 film preparation, device fabrication, and the photocurrent–voltage measurements were as reported in our earlier publication [6a]. The volatile electrolyte (Z675) contains 1.0 M PMII, 0.03 M iodine, 0.1 M GuNCS, and 0.5 M *tert*-butylpyridine in acetonitrile and valeronitrile (3:1 v/v). The nonvolatile electrolyte (Z646) contains 1.0 M PMII, 0.15 M iodine, 0.1 M GuNCS, and 0.5 M NBB in 3-methoxypropionitrile.

Received: September 22, 2006
Revised: February 13, 2007

[1] M. Grätzel, *Nature* **2001**, *414*, 338.
[2] B. O'Regan, M. Grätzel, *Nature* **1991**, *353*, 737.
[3] M. Grätzel, *Chem. Lett.* **2005**, *34*, 8.
[4] M. Grätzel, *Inorg. Chem.* **2005**, *44*, 6841.
[5] a) K. D. Benkstein, N. Kopidakis, J. van de Lagemaat, A. J. Frank, *J. Phys. Chem. B* **2003**, *107*, 7759. b) G. Benkö, B. Skårman, R. Wallenberg, A. Hagfeldt, V. Sundström, A. P. Yartsev, *J. Phys. Chem. B* **2003**, *107*, 1370. c) S. Nakade, Y. Saito, W. Kubo, T. Kitamura, Y. Wada, S. Yanagida, *J. Phys. Chem. B* **2003**, *107*, 8607.
[6] a) D. Kuang, S. Ito, B. Wenger, C. Klein, J.-E. Moser, R. Humphry-Baker, S. M. Zakeeruddin, M. Grätzel, *J. Am. Chem. Soc.* **2006**, *128*, 4146. b) D. Kuang, C. Klein, H. J. Snaith, J. E. Moser, R. Humphry-Baker, P. Comte, S. M. Zakeeruddin, M. Grätzel, *Nano Lett.* **2006**, *6*, 769. c) P. Wang, C. Klein, R. Humphry-Baker, S. M. Zakeeruddin, M. Grätzel, *J. Am. Chem. Soc.* **2005**, *127*, 808. d) P. Wang, C. Klein, R. Humphry-Baker, S. M. Zakeeruddin, M. Grätzel, *Appl. Phys. Lett.* **2005**, *86*, 123 508. e) D. Kuang, C. Klein, S. Ito, J.-E. Moser, R. Humphry-Baker, S. M. Zakeeruddin, M. Grätzel, *Adv. Funct. Mater.* **2007**, *17*, 154.
[7] a) D. Kuang, P. Wang, S. Ito, S. M. Zakeeruddin, M. Grätzel, *J. Am. Chem. Soc.* **2006**, *128*, 7732. b) H. X. Wang, H. Li, B. F. Xue, Z. X. Wang, Q. B. Meng, L. Q. Chen, *J. Am. Chem. Soc.* **2005**, *127*, 6394. c) M. Yanagida, T. Yamaguchi, M. Kurashige, G. Fujihashi, K. Hara, R. Katoh, H. Sugihara, H. Arakawa, *Inorg. Chim. Acta* **2003**, *351*,

283. d) V. Balzani, S. Campagna, G. Denti, A. Juris, S. Serroni, M. Venturi, *Acc. Chem. Res.* **1998**, *31*, 26. e) K. Hara, M. Kurashige, Y. Dan-oh, C. Kasada, A. Shinpo, S. Suga, K. Sayama, H. Arakawa, *New J. Chem.* **2003**, 783. f) T. Horiuchi, H. Miura, S. Uchida, *Chem. Commun.* **2003**, 3036.

[8] a) M. K. Nazeeruddin, P. Pechy, T. Renouard, S. M. Zakeeruddin, R. Humphry-Baker, P. Liska, L. Cevey, E. Costa, V. Shklover, L. Spiccia, G. B. Deacon, C. A. Bignozzi, M. Grätzel, *J. Am. Chem. Soc.* **2001**, *123*, 1613. b) V. Aranyos, J. Hjelm, A. Hagfeldt, H. Grennberg, *J. Chem. Soc., Dalton Trans.* **2003**, 1280.

[9] a) K. Hara, M. Kurashige, Y. Kan-oh, C. Kasada, A. Shinpo, S. Suga, K. Sayama, H. Arakawa, *New J. Chem.* **2003**, *27*, 783. b) T. Horiuchi, H. Miura, K. Sumioka, S. Uchida, *J. Am. Chem. Soc.* **2004**, *126*, 12 218.

[10] a) M. Adachi, Y. Murata, J. Takao, J. Jiu, M. Sakamoto, F. Wang, *J. Am. Chem. Soc.* **2004**, *126*, 14 943. b) M. Zukalova, A. Zukal, L. Kavan, M. K. Nazeeruddin, P. Lisa, M. Grätzel, *Nano Lett.* **2005**, *5*, 1789. c) H. Lindström, A. Holmberg, E. Magnusson, S. E. Lindquist, L. Malmqvist, A. Hagfeldt, *Nano Lett.* **2001**, *1*, 97.

[11] a) J. Bisquert, *J. Phys. Chem. B* **2002**, *106*, 325. b) J. Bisquert, *Phys. Chem. Chem. Phys.* **2003**, *5*, 5360. c) J. van de Lagemaat, N.-G. Park, A. J. Frank, *J. Phys. Chem. B* **2000**, *104*, 2044. d) J. Bisquert, A. Zaban, M. Greenshtein, I. Mora-Sero, *J. Am. Chem. Soc.* **2004**, *126*, 13 550. e) F. Fabregat-Santiago, J. Bisquert, G. Garcia-Belmonte, G. Boschloo, A. Hagfeldt, *Sol. Energy Mater. Sol. Cells* **2005**, *87*, 117.

[12] Q. Wang, J. E. Moser, M. Grätzel, *J. Phys. Chem. B* **2005**, *109*, 14 945.

[13] P. Bonhôte, A.-P. Dias, N. Papageorgiou, K. Kalyanasundaram, M. Grätzel, *Inorg. Chem.* **1996**, *35*, 1168.

[14] Z.-G. Le, Z.-C. Chen, Y. Hu, Q.-G. Zheng, *Synthesis* **2004**, 208.

